arXiv:2505.09252v1 [cs.CV] 14 May 2025

Zero-Shot Multi-modal Large Language Models v.s. Supervised Deep Learning: A Comparative Study on CT-Based Intracranial Hemorrhage Subtyping

Yinuo Wang[a], Yue Zeng[a], Kai Chen[b], Cai Meng[a], Chao Pan[c], Zhouping Tang[c]

[a]*Image Processing Center, Beihang University, Beijing 100191, China*
[b]*School of Mechanical Engineering and Automation, Beihang University, Beijing 100191, China*
[c]*Department of Neurology, Tongji Hospital, Tongji Medical College, Huazhong University of Science and Technology, Wuhan 430030, China*

Abstract

Introduction: Timely identification of intracranial hemorrhage (ICH) subtypes on non-contrast computed tomography is critical for prognosis prediction and therapeutic decision-making, yet remains challenging due to low contrast and blurring boundaries. This study evaluates the performance of zero-shot multi-modal large language models (MLLMs) compared to traditional deep learning methods in ICH binary classification and subtyping. **Methods:** We utilized a dataset provided by RSNA, comprising 192 NCCT volumes. The study compares various MLLMs, including GPT-4o, Gemini 2.0 Flash, and Claude 3.5 Sonnet V2, with conventional deep learning models, including ResNet50 and Vision Transformer. Carefully crafted prompts were used to guide MLLMs in tasks such as ICH presence, subtype classification, localization, and volume estimation. **Results:** The results indicate that in the ICH binary classification task, traditional deep learning models outperform MLLMs comprehensively. For subtype classification, MLLMs also exhibit inferior performance compared to traditional deep learning models, with Gemini 2.0 Flash achieving an macro-averaged precision of 0.41 and a macro-averaged F1 score of 0.31. **Conclusion:** While MLLMs excel in interactive capabilities, their overall accuracy in ICH subtyping is inferior to deep networks. However, MLLMs enhance interpretability through lan-

Corresponding author: Cai Meng

guage interactions, indicating potential in medical imaging analysis. Future efforts will focus on model refinement and developing more precise MLLMs to improve performance in three-dimensional medical image processing.

Keywords: Intracranial hemorrhage subtyping, multi-modal large language models, medical image classification, validation.

1. Introduction

Intracranial hemorrhage (ICH) is a life-threatening acute cerebrovascular disease, affecting approximately 2 million individuals worldwide each year. Despite advances in medical care, the 30-day mortality rate remains exceptionally high, ranging between 35% and 52%, with only one-fifth of survivors achieving complete recovery within six months post-onset [1, 2]. The etiology of ICH is multifactorial, commonly associated with external trauma, hypertension, thrombosis, neoplasms, or vascular malformations [3]. These underlying causes can lead to one or more subtypes of hemorrhage, which are typically classified by location into epidural hemorrhage (EDH), intraparenchymal hemorrhage (IPH), intraventricular hemorrhage (IVH), subarachnoid hemorrhage (SAH), and subdural hemorrhage (SDH) [4]. During the acute phase of ICH, non-contrast computed tomography (NCCT) scans are widely used to detect and characterize specific hemorrhage subtypes, facilitating the development of timely and personalized treatment strategies. Moreover, NCCT imaging remains essential during surgical procedures and follow-up evaluations to assess residual hemorrhage and monitor the recovery process [5, 6]. Therefore, the rapid and accurate identification of ICH and its subtypes based on NCCT is critical for hospitals worldwide. This is particularly challenging in resource-limited settings, where access to highly experienced clinicians and advanced imaging technologies is often restricted.

The detection of ICH subtypes is typically complicated by the variability in the shape, size, and contrast with surrounding soft tissues. This variability increases the risk of missed or incorrect diagnoses during NCCT evaluations. Furthermore, studies have demonstrated notable inter-observer variability among radiologists with varying levels of expertise, which negatively impacts patient management and clinical outcomes [8]. In recent years, advancements in artificial intelligence have driven the development of deep learning methods for ICH subtype diagnosis. Early approaches utilized convolutional neural networks (CNNs) to extract low-level features from slices

[10, 11, 12, 13, 14, 15]. Lee et al. emulated the diagnostic workflow of radiologists by implementing multi-window conversion and slice interpolation as preprocessing steps for NCCT scans. They incorporated pretrained CNNs for ICH subtype prediction, complemented by attention maps to enhance the interpretability of predictions [10]. Ye et al. developed a joint CNN-RNN classification framework, which used a CNN to extract slice-level features and an RNN to model contextual relationships across slices. The framework first performed binary ICH detection, followed by five-class subtype classification on positive samples to identify the specific ICH subtypes present [11]. Subsequent research has advanced classification methodologies through multiple directions. Notably, Vision Transformers (ViTs) have been increasingly adopted as backbone architectures to replace conventional CNNs, demonstrating enhanced non-local feature representation capabilities in medical imaging tasks [16]. To address computational constraints, lightweight modules have been developed, achieving comparable accuracy with reduced parameters [17]. The integration of attention mechanisms has further improved model performance by selectively focusing on pathologically significant regions [14, 19]. Technical refinements in preprocessing pipelines, particularly artifact reduction strategies, have enhanced ICH detection accuracy through minimized noise interference [18]. Meanwhile, semi-supervised learning frameworks leveraging unlabeled datasets effectively mitigate data scarcity challenges while maintaining diagnostic robustness [20]. These synergistic advancements collectively contribute to more reliable and deployable computer-aided ICH diagnosis systems.

Despite significant advancements in classification and detection accuracy, these primary automated methods predominantly generates elementary outputs of predicted classifications or detection results, failing to interact with human like a reliable expert. That means, when an ICH subtype is recognized by these methods, radiologists must still meticulously analyze and assess bleeding volume, severity, treatment options, and other abnormalities, which continues to demand clinical expertise and labor-intensive scrutiny from medical personnel. With the advent of artificial general intelligence (AGI), multi-modal large language models (MLLMs) are poised to revolutionize radiology workflows. These systems synergize robust visual processing with natural language capabilities that encapsulate accumulated diverse medical knowledge, thereby enabling intuitive interaction between generalized AI models and end users [21, 22]. Across diverse medical applications, MLLMs demonstrate the capacity to provide valuable differential diagnoses

from input images, generate preliminary structured reports, characterize lesions, evaluate disease burden, and recommend appropriate treatment and follow-up protocols [23, 24, 25, 26, 27]. These capabilities can assist radiologists in triage, prioritization, and decision-support processes. Within this context, our research aims to evaluate the efficacy of contemporary MLLMs in identifying ICH subtypes. In this study, we emulate the diagnostic process of neurosurgeons by inputting windowed NCCT slices alongside progressive prompts to guide MLLMs in predicting ICH presence, subtype classification, localization, hemorrhage volume, treatment recommendations, and other potential abnormalities. A comprehensively annotated dataset comprising 192 NCCT scans with 6,404 slices was partitioned into training, validation, and testing subsets. Our evaluation on the test set encompasses not only proprietary MLLMs and more lightweight, deployable open-source alternatives but also incorporates comparative analysis with conventional deep learning classification models based on CNNs and transformer architectures.

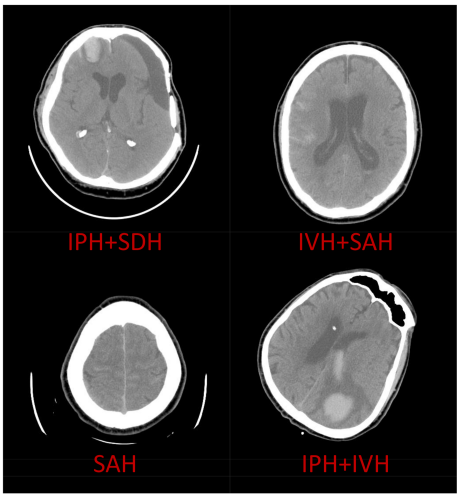
2. Methods

2.1. Data Usage

We employed a subset of the brain hemorrhage dataset originally provided by the Radiological Society of North America (RSNA). The dataset was initially released as randomly ordered DICOM-format slices. Wu et al. [33] reconstructed 192 NCCT volumes, each containing one or more subtypes of ICH, by leveraging anonymized patient identifiers and geometric/positional metadata embedded in the DICOM files. These volumes were subsequently annotated at the pixel level by two medical imaging experts and radiology residents. The annotation process was guided by the original slice-level hemorrhage annotations and included five ICH subtypes: EDH, IPH, IVH, SAH, and SDH. The dataset was made available under the MIT License. During preprocessing, windowing was applied to the volumes with a window width of 200 and a window level of 20. Slices above the cranial vertex that lacked intracranial tissue were excluded, and the remaining slices were converted to PNG format. For experimental purposes, 10% of the slices were randomly selected to create the test set, resulting in a total of 561 slices.

2.2. Prompt Usage

Prompts act as a pivotal mechanism connecting user intent with model capabilities in large language models (LLMs), directing the generation of



(a)

Please assume the role of both a radiology and neurosurgery expert. I will input a brain CT slice with a window width of 200 HU and a window level of 20 HU. This slice may or may not contain intracranial hemorrhage, and if present, it may include one or more subtypes of hemorrhage. After reviewing the slice, please answer the following questions:
1. Which part of the brain is depicted in this slice?
2. Is there any evidence of intracranial hemorrhage in this slice? Please answer with "Yes" or "No."
3. If intracranial hemorrhage is present, please specify which hemorrhage subtypes are observed. The known subtypes of hemorrhage include: extradural hemorrhage (EDH), subdural hematoma (SDH), subarachnoid hemorrhage (SAH), intraparenchymal hemorrhage (IPH), and intraventricular hemorrhage (IVH). If no hemorrhage is present, please respond with "None."
4. If intracranial hemorrhage is present, please locate the hemorrhage and quantify the hemorrhage volume in each observed subtype. (Assume that one pixel in the image represents a hemorrhage volume of 1 unit.) If no hemorrhage is present, please respond with "None."
5. If intracranial hemorrhage is present, what is your treatment recommendation? Choose between conservative treatment or puncture therapy. If no hemorrhage is present, please respond with "None."
6. Are there any other abnormalities observed in this slice? If yes, please describe them. If no, please respond with "None."

(b)

Figure 1: (a) Random samples from the utilized dataset, with hemorrhage subtypes labeled in red; (b) The designed prompt.

desired outputs through carefully crafted contextual cues [34, 35]. In multimodal applications, prompts leverage cross-modal information, such as text and images, to expand the model's ability to generalize across complex tasks. Moreover, task-specific prompt designs can substantially enhance output quality by achieving an optimal balance between factual accuracy, creativity, and controllability.

This study introduces a progressive prompt design for the cases, as depicted in Fig. 1 b. Building on prior prompting methodologies (citation), we initially assigned specific roles to the MLLMs to activate their domain-specific knowledge, instructing them to "act as a radiology expert and a neurosurgery specialist." Following the introduction of task-relevant context, the first question focused on identifying the brain region represented in the given slice, aimed at evaluating the MLLMs' scene comprehension capabilities. The second question examined the presence of intracranial hemorrhage within the slice, framing the task as a binary classification problem. The third question expanded upon the second, requiring the MLLMs to iden-

tify the subtype of intracranial hemorrhage if detected. The fourth question further progressed by instructing the MLLMs to localize the hemorrhage area and quantify its volume. The final two questions shifted toward clinical decision-making and anomaly detection. Specifically, they assessed the MLLMs' preferences for treatment recommendations and their ability to recognize potential disease threats. These conclusions, designed as open-ended interactions, lacked ground truth comparisons, allowing for exploratory evaluation. This progressive prompt design aimed to systematically assess the MLLMs' capabilities across binary classification, multi-class classification, localization, and quantification tasks related to intracranial hemorrhages. Furthermore, the open-ended interactions were intended to explore the MLLMs' reasoning concerning the intrinsic links between diagnostic processes and clinical decision-making.

2.3. Multi-Modal Large Language Models (MLLMs)

This study employed both proprietary and open-source MLLMs. The proprietary models include GPT-4o, Gemini 2.0 Flash, and Claude 3.5 Sonnet V2, while the open-source models comprise Qwen-VL-3b-Instruct, DeepSeek-VL2-Tiny, and LLaVA-Med-v1.5-Mistral-7b. GPT-4o was developed by OpenAI and released in May 2024, Gemini 2.0 Flash by Google in January 2025, and Claude 3.5 Sonnet V2 by Anthropic in October 2024. For the open-source models, Qwen-VL-3b-Instruct was launched by Alibaba Cloud in February 2025, DeepSeek-VL2-Tiny by DeepSeek in December 2024, and LLaVA-Med-v1.5-Mistral-7b by Microsoft in May 2024. Notably, LLaVA-Med-v1.5-Mistral-7b is specifically tailored for applications in the biomedicine domain, whereas the other models are designed for general-domain tasks.

During the evaluation phase, GPT-4o, Gemini 2.0 Flash, and Claude 3.5 Sonnet V2 were accessed through their respective application programming interfaces (APIs), while Qwen-VL-3b-Instruct, DeepSeek-VL2-Tiny, and LLaVA-Med-v1.5-Mistral-7b were deployed locally on a server equipped with four Nvidia RTX 3090 GPUs. To ensure consistent and deterministic outputs, the temperature parameter for all models was set to 0.1.

2.4. Learning-Based Classifiers

To comprehensively assess the classification performance of MLLMs, we incorporated commonly used image classification models based on CNNs and

Transformers, including ResNet50, ViT-B, ViT-L, and SwinTransformer-v2-B. For intracranial hemorrhage classification tasks, encompassing binary classification and subtype recognition, all models were trained under a unified strategy. Specifically, slices excluded from the test set were partitioned into training and validation sets in an 8:2 ratio. The training process was performed for 100 epochs, employing the cross-entropy loss function, Adam optimizer, a learning rate of 10^{-4}, and a batch size of 32. To enhance model generalization, data augmentation techniques such as random flipping and rotation were applied. For the subtype recognition task, we utilized the multi-label binary cross-entropy loss function (log-loss), which is defined as follows:

$$\mathcal{L} = -\frac{1}{K}\frac{1}{C}\sum_{k=1}^{K}\sum_{c=1}^{C}\left[y_{c,k}\log(\hat{y}_{c,k}) + (1-y_{c,k})\log(1-\hat{y}_{c,k})\right] \tag{1}$$

where K and C denotes the number of training samples and classes, respectively. C equals to 5 in our work, including five ICH subtypes. $y_{c,k}$ represents the ground truth label of the k-th sample for the c-th class, and $\hat{y}_{c,k}$ represents the predicted ICH subtype probabilities.

3. Results

3.1. Performance of ICH Binary Classification

Initially, we assessed the performance of models on the ICH binary classification task. As depicted in Table 1, among proprietary MLLMs, GPT-4o and Gemini 2.0 Flash generally outperformed Claude 3.5 Sonnet V2. Specifically, Gemini 2.0 Flash exceeded GPT-4o in Accuracy, Precision, and Specificity approximately by 0.05, 0.16, and 0.17, respectively. In contrast, GPT-4o demonstrated superior Sensitivity and F1 score, leading by 0.11 and 0.002, respectively. These results suggest that Gemini 2.0 Flash is more adept at identifying healthy cases and reducing false positives, whereas GPT-4o offers better coverage for hemorrhage cases, albeit with increased false alarms. Conversely, the included open-source MLLMs exhibited inferior overall performance compared to proprietary MLLMs. Despite achieving higher sensitivity rates, their peak accuracy, precision, specificity, and F1 scores were substantially lower. Notably, models such as Qwen-VL-3B-Instruct and DeepSeek-VL2-tiny showed low Specificity and high Sensitivity, resulting in a high rate of false positive predictions and indicating their limited ability to effectively

Table 1: Quantitative comparison of ICH binary classification on the testing datasets. **Bold** text denotes the best performance in each group of methods.

Methods	Accuracy	Precision	Sensitivity	Specificity	F1 score
Proprietary					
GPT-4o	0.7005	0.6390	**0.6553**	0.7331	**0.6471**
Gemini 2.0 Flash	**0.7504**	**0.7987**	0.5404	**0.9018**	0.6447
Claude 3.5 Sonnet V2	0.6275	0.5489	0.6213	0.6319	0.5828
Open-source					
Qwen-VL-3b-Instruct	0.4385	0.4231	0.9362	0.0798	0.5828
DeepSeek-VL2-Tiny	0.4225	0.4204	**1.0000**	0.0061	**0.5919**
LLaVA-Med-v1.5-Mistral-7b	**0.4955**	**0.4358**	0.6936	**0.3528**	0.5353
Classifiers					
ResNet50	0.8966	0.8734	**0.8809**	0.9080	0.8771
ViT-B	0.8556	0.8702	0.7702	0.9171	0.8172
ViT-L	0.8770	0.8517	0.8553	0.8926	0.8535
SwinTransformer-v2-B	**0.9091**	**0.9035**	0.8766	**0.9325**	**0.8898**

distinguish hemorrhagic features. Furthermore, classifiers trained on ICH datasets consistently outperformed MLLMs across all evaluated metrics except Sensitivity. This indicates that while MLLMs have advanced interactive capabilities, their visual classification performance is still lacking compared to deep networks trained on specialized data, primarily due to insufficient generalization in hemorrhage detection tasks.

3.2. Performance of ICH Subtype Classification

Table 2 presents the macro-average results of ten methods in classifying five intracranial hemorrhage (ICH) subtypes. In this task, MLLMs consistently underperform compared to learning-based classifiers. Among proprietary MLLMs, Gemini 2.0 Flash demonstrates the highest overall performance. However, it exhibits reductions of approximately 0.47 in Precision, 0.55 in Sensitivity, 0.03 in Specificity, and 0.55 in F1 score when compared to SwinTransformer-v2-B. This suggests that while proprietary MLLMs tend to generate fewer false positives, their proficiency in subtype identification is still limited. Notably in these comparisons, proprietary MLLMs generally surpass open-source MLLMs in performance. Fig. 2 provides an independent analysis of ten methods for identifying the five subtypes. In terms of

Table 2: Quantitative comparison of ICH subtype classification on the testing datasets. The results for the five subtypes are calculated using macro-averaging. **Bold** text denotes the best performance in each group of methods.

Methods	Precision	Sensitivity	Specificity	F1 score
Proprietary				
GPT-4o	0.3243	0.2734	0.9232	0.2842
Gemini 2.0 Flash	**0.4093**	**0.2909**	**0.9526**	**0.3116**
Claude 3.5 Sonnet V2	0.2459	0.2169	0.9091	0.2282
Open-source				
Qwen-VL-3b-Instruct	**0.1069**	0.3393	0.6442	0.1524
DeepSeek-VL2-Tiny	0.0997	**0.6366**	0.3281	**0.1547**
LLaVA-Med-v1.5-Mistral-7b	0.1035	0.2682	**0.7438**	0.1393
Classifiers				
ResNet50	0.8488	**0.8542**	0.9765	0.8512
ViT-B	0.7964	0.8065	0.9705	0.8001
ViT-L	0.8056	0.8113	0.9730	0.8071
SwinTransformer-v2-B	**0.8782**	0.8384	**0.9799**	**0.8569**

Sensitivity, MLLMs exhibit a significant decline compared to learning-based classifiers for EDH, IVH, and SAH, while the disparity is less pronounced for IPH and SDH. Regarding Specificity, proprietary MLLMs and learning-based classifiers show comparable performance across all five subtypes, aligning with observations in Table 2. For the F1 score, proprietary MLLMs excel in IPH but perform less effectively for EDH and SAH.

3.3. Open-ended Analysis

This section compares the responses of six MLLMs on specific cases to assess the comprehensiveness and reasoning of their answers. Fig. 3 illustrates an IPH in the right hemisphere and an SDH in the left hemisphere on the input slice. For this case, all MLLMs successfully detected the presence of hemorrhage (the second answer), but only LLaVA-Med-v1.5-Mistral-7b accurately identified the ICH subtypes (the third answer). Concerning the fourth question about hemorrhage volume, the ground truth annotations for IPH and SDH are 1600 and 5761 units, respectively. Only Gemini 2.0 Flash

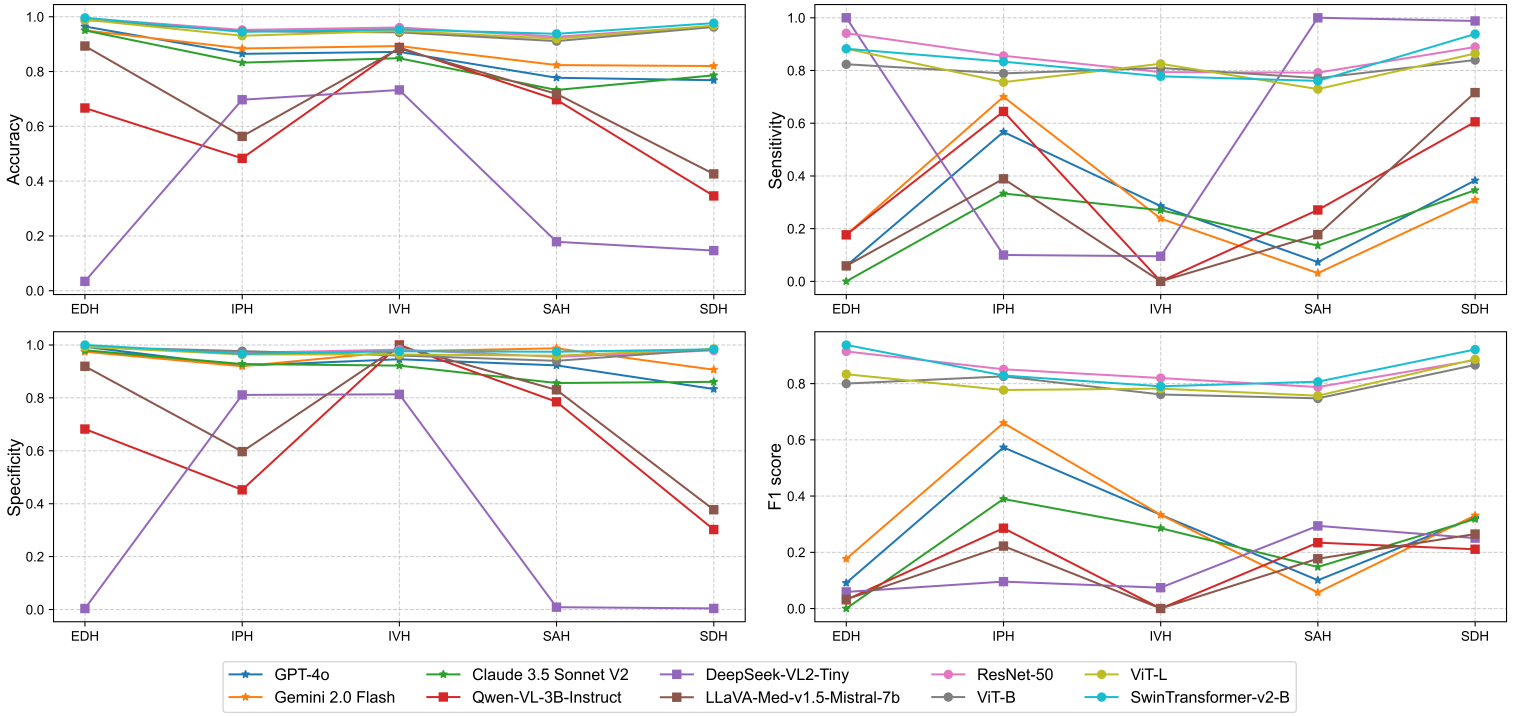


Figure 2: Line chart showing the performance of various models in the recognition of ICH subtypes.

provided estimates within the correct order of magnitude but mistakenly identified IPH as EDH. For treatment recommendations in the fifth question, the models proposed various options: Gemini 2.0 Flash suggested puncture therapy, while Claude 3.5 Sonnet v2, Qwen-VL-3b-Instruct, and LLaVA-Med-v1.5-Mistral-7b recommended conservative treatment. GPT-4o advised conservative treatment for IVH and puncture therapy for SDH. Additionally, GPT-4o, Gemini 2.0 Flash, and Claude 3.5 Sonnet v2 reported observed abnormalities, such as midline shift, whereas the other three models reported no abnormalities. Overall, GPT-4o, Gemini 2.0 Flash, and Claude 3.5 Sonnet v2 provided more comprehensive and reasonably coherent responses to open-ended questions, while DeepSeek-VL2-Tiny's responses to questions three through five lacked coherence.

4. Discussions

This prehospital study assessed the effectiveness of various MLLMs in identifying ICH subtypes. The results reveal that mainstream MLLMs, both proprietary and open-source, fall short in classification performance compared to trained classifiers. Proprietary MLLMs notably outperform open-source ones, likely due to the smaller parameter size of deployable MLLMs utilized in this study. Comparative analysis of Table 1 and Table 2 demonstrates that MLLMs are significantly less effective in recognizing ICH subtypes than in detecting general hemorrhages. This indicates that while MLLMs possess basic hemorrhage detection capabilities, they lack the ability to discern and learn specific subtype characteristics. Our observations suggest that the accuracy of MLLMs in identifying ICH correlates with the contrast and size of the lesion, consistent with intuitive principles of image processing. Fig. 4 illustrates two cases from different slices of the same NCCT volume, where the contrast of IPH lesion in the left image is lower than in the right. Consequently, GPT-4o failed to accurately detect the ICH and IPH subtype in the left image but successfully identified the lesion in the right image. As depicted in Fig. 5, the performance of three proprietary MLLMs improves as the size of the hemorrhage region increases. This suggests that current MLLMs have limited screening capabilities for small lesions across various ICH subtypes and underscores the disparity in MLLMs' ability to recognize different ICH subtypes. Specifically, they are more proficient in identifying IPH with higher edge contrast and concentrated lesions, whereas their performance declines in recognizing SAH with lower contrast and more dispersed lesions. Furthermore, when slices contain metal objects or calcifications, MLLMs are prone to misinterpret them as hemorrhages. Additionally, metal artifacts can lead MLLMs to misclassify positive cases as normal due to difficulties in distinguishing visual illusions caused by the artifacts, resulting in misjudgment. Overall, the predictive accuracy of MLLMs in ICH subtype classification remains significantly lower than that of trained deep classification networks. However, MLLMs can enhance interpretability through language interactions, such as describing hemorrhage locations, offering treatment suggestions, and noting abnormalities. Future fine-tuning of open-source models is expected to improve their performance, potentially contributing positively to triage, examination, monitoring, and prognosis in ICH management [36].

5. Limitation

This study has two main limitations. Firstly, due to hardware resource constraints, we utilized open-source models with relatively small parameter sizes within their respective series. This may hinder these models from fully leveraging their potential in ICH subtype classification tasks. Secondly, due to the current limitations of MLLMs, our hemorrhage subtype prediction analysis was restricted to 2D slices, potentially causing certain cranial structures to be misidentified as high-density hemorrhage areas. Therefore, advancing high-precision MLLMs capable of volumetric medical image processing is a vital direction for future research. In upcoming work, we aim to develop a structured image-text dataset specifically for ICH subtype classification and investigate the fine-tuning of MLLMs for this task to further improve their performance.

6. Conclusions

This study compares multi-modal large language models (MLLMs) to traditional deep learning methods in intracranial hemorrhage (ICH) subtyping. The findings reveal that although MLLMs excel in certain tasks, their overall accuracy is inferior to deep learning models. Nevertheless, MLLMs enhance interpretability through language interactions, indicating potential in medical imaging analysis. Future efforts will focus on model fine-tuning and developing more precise MLLMs to improve performance in volumetric ICH subtyping.

7. Code Availability

The preprocessing data and code used in this research are available on GitHub (`https://github.com/mileswyn/ICH_MLLMs_validation`).

8. Acknowledgments

This work was supported in part by the National Natural Science Foundation of China under Grants (92148206).

References

[1] C. J. J. van Asch, M. J. A. Luitse, G. J. E. Rinkel, I. V. D. Tweel, A. Algra, and C. J. M. Klijn, *"Incidence, Case Fatality, and Functional Outcome of Intracerebral Haemorrhage over Time, According to Age, Sex, and Ethnic Origin: A Systematic Review and Meta-Analysis."* The Lancet Neurology, 9(2), 167-176, 2010.

[2] O. Adeoye, and J. P. Broderick, *"Advances in the Management of Intracerebral Hemorrhage."* Nature Reviews Neurology, 6(11), 593-601, 2010.

[3] C. Cordonnier, A. Demchuk, W. Ziai, and C. S. Anderson, *"Intracerebral Haemorrhage: Current Approaches to Acute Management."* The Lancet, 392(10154), 1257-1268, 2018.

[4] S. R. Martini, M. L. Flaherty, W. M. Brown, M. Haverbusch, M. E. Comeau, L. R. Sauerbeck, B. M. Kissela, R. Deka, D. O. Kleindorfer, C. J. Moomaw, J. P. Broderick, C. D. Langefeld, and D. Woo, *"Risk Factors for Intracerebral Hemorrhage Differ According to Hemorrhage Location."* Neurology, 79(23), 2275-2282, 2012.

[5] F. Macellari, M. Paciaroni, G. Agnelli, and V. Caso, *"Neuroimaging in Intracerebral Hemorrhage."* Stroke, 45(3), 903-908, 2014.

[6] W. Jia, B. Zhao, J. Du, G. Wu, and T. Wang, *"Identifying the Specific Subtype of Intracerebral Hemorrhage That Is Indicated for Minimally Invasive Craniopuncture."* Neurocritical care, 33, 670-678, 2020.

[7] O. R. Karam, O. A. de Andrade Leão, A. E. Martio, J. R. Vanzin, and P. M. Mesquita Filho, *"Chronic Subdural Hematoma: Epidemiological Analysis and Factors Associated with Hematoma Size – A Single Center Experience."* Brain Hemorrhages, 5(4), 177-180.

[8] W. M. Strub, J. L. Leach, T. Tomsick, and A. Vagal, *"Overnight Preliminary Head CT Interpretations Provided by Residents: Location of Misidentified Intracranial Hemorrhage."* Nature Reviews Neurology, 6(11), 593-601, 2010.

[9] S. Chilamkurthy, R. Ghosh, S. Tanamala, M. Biviji, N. G. Campeau, V. K. Venugopal, V. Mahajan, P. Rao, and P. Warier, *"Deep Learning*

Algorithms for Detection of Critical Findings in Head CT Scans: A Retrospective Study." The Lancet, 392(10162), 2388-2396, 2018.

[10] H. Lee, S. Yune, M. Mansouri, M. Kim, S. H. Tajmir, C. E. Guerrier, S. A. Ebert, S. R. Pomerantz, J. M. Romero, S. Kamalian, R. G. Gonzalez, M. H. Lev and S. Do, *"An Explainable Deep-Learning Algorithm for The Detection of Acute Intracranial Haemorrhage from Small Datasets."* Nature Biomedical Engineering, 3, 173-182, 2019.

[11] H. Ye, F. Gao, Y. Yin, D. Guo, P. Zhao, Y, Lu, X. Wang, J. Bai, K. Cao, Q. Song, H. Zhang, W. Chen, X. Guo, and J. Xia, *"Precise Diagnosis of Intracranial Hemorrhage and Subtypes Using A Three-Dimentional Joint Convolutional and Recurrent Neural Network."* European Radiology, 29, 6191-6201, 2019.

[12] Y. Wu, M. P. Supanich, and J. Deng, *"Ensembled Deep Neural Network for Intracranial Hemorrhage Detection and Subtype Classification on Noncontrast CT Images."* Journal of Artificial Intelligence for Medical Sciences, 2(1-2), 12-20, 2021.

[13] X. Wang, T. Shen, S. Yang, J. Lan, Y. Xu, M. Wang, J. Zhang, and X. Han, *"A Deep Learning Algorithm for Automatic Detection and Classification of Acute Intracranial Hemorrhages in Head CT Scans."* NeuroImage: Clincal, 32, 102785, 2021.

[14] D. Alis, C. Alis, M. Yergin, C. Topel, O. Asmakutlu, O. Bagcilar, Y. D. Senli, A. Ustundag, V. Salt, S. N. Dogan, M. Velioglu, H. H. Selcuk, B. Kara, C. Ozer, I. Oksuz, O. Kizilkilic, and E. Karaarslan, *"A Joint Convolutional-Recurrent Neural Network with An Attention Mechanism for Detecting Intracranial Hemorrhage on Noncontrast Head CT."* Scientific Reports, 12(1), 2084, 2022.

[15] M. Yeo, B. Tahayori, H. K. Kok, J. Maingard, N. Kutaiba, J. Russell, V. Thijs, A. Jhamb, R. V. Chandra, M. Brooks, C. D. Barras, and H. Asadi, *"Evaluation of Techniques to Improve A Deep Learning Algorithm for The Automatic Detection of Intracranial Haemorrhage on CT Head Imaging."* European Radiology Experimental, 7(1), 17, 2023.

[16] Y. Wang, A. Stefanidis, and J. Liu, *"Multi-Stage Transformer Fusion for Efficient Intracranial Hemorrhage Subtype Classification."* 2024 IEEE International Symposium on Biomedical Imaging (ISBI), 1-5, 2024.

[17] Y. Chen, C. Chen, C. Kuo, and C. Lin, *"An Efficient Deep Neural Network for Automatic Classification of Acute Intracranial Hemorrhages in Brain CT Scans."* Computers in Biology and Medicine, 176, 108587, 2024.

[18] J. Thalhammer, M. Schultheiß, T. Dorosti, T. Lasser, F. Pfeiffer, D. Pfeiffer, and F. Schaff, *"Improving Automated Hemorrhage Detection at Sparse-View CT via U-Net-Based Artifact Reduction."* Radiology: Artificial Intelligence, 6(4), e230275, 2024.

[19] L. P. Kothala, and S. R. Guntur, *"GEL-TTA Net: A Global Ensemble Learning Network for The Localization of Small-Scale and Mixed Intracranial Hemorrhages Through Test Time Augmentations."* Multimedia Tools and Applications, 6(4), e230275, 2024.

[20] E. Lin, E. L. Yuh *"Semi-Supervised Learning for Generalizable Intracranial Hemorrhage Detection and Segmentation."* Radiology: Artificial Intelligence, 6(3), e230077, 2024

[21] X. Yue, Y. Ni, K. Zhang, T. Zheng, R. Liu, G. Zhang, S. Stevens, D. Jiang, W. Ren, Y. Sun, C. Wei, B. Yu, R. Yuan, R. Sun, M. Yin, B. Zheng, Z. Yang, Y. Liu, W. Huang, H. Sun, Y. Su, and W. Chen, *"MMMU: A Massive Multi-Discipline Multimodal Understanding and Reasoning Benchmark for Expert AGI."* Proceedings of the IEEE/CVF Conference on Computer Vision and Pattern Recognition, 2024, 9556-9567.

[22] T. Li, Y. Su, W. Li, B. Fu, Z. Chen, Z. Huang, G. Wang, C. Ma, Y. Chen, M. Hu, Y. Li, P. Chen, X. Hu, Z. Deng, Y. Ji, J. Ye, Y. Qiao, and J. He, *"GMAI-VL & GMAI-VL-5.5M: A Large Vision-Language Model and A Comprehensive Multimodal Dataset Towards General Medical AI."* arXiv preprint arXiv: 2411.14522, 2024.

[23] F. Liu, T. Zhu, X. Wu, B. Yang, C. You, C. Wang, L. Lu, Z. Liu, Y. Zheng, X. Sun, Y. Yang, L. Clifton, and D. A. Clifton, *"A Medical Multimodal Large Language Model for Future Pandemics."* NPJ Digital Medicine, 6(1), 226, 2023.

[24] T. Li, Y. Su, W. Li, B. Fu, Z. Chen, Z. Huang, G. Wang, C. Ma, Y. Chen, M. Hu, Y. Li, P. Chen, X. Hu, Z. Deng, Y. Ji, J. Ye, Y. Qiao, and

J. He, *"A Generalist Vision-Language Foundation Model for Diverse Biomedical Tasks."* Nature Medicine, 30, 3129-3141, 2024.

[25] M. Y. Lu, B. Chen, D. F. K. Williamson, R. J. Chen, M. Zhao, A. K. Chow, K. Ikemura, A. Kim, D. Pouli, A. Patel, A. Soliman, C. Chen, T. Ding, J. J. Wang, G. Gerber, I. Liang, L. P. Le, A. V. Parwani, L. L. Weishaupt, and F. Mahmood, *"A Multimodal Generative AI Copilot for Human Pathology."* Nature, 634(8033), 466-473, 2024.

[26] J. Xiang, X. Wang, X. Zhang, Y. Xi, F. Eweje, Y. Chen, Y. Li, C. Bergstrom, M. Gopaulchan, T. Kim, K. Yu, S. Willens, F. M. Olguin, J. J. Nirschl, J. Neal, M. Diehn, S. Yang, and R. Li, *"A Vision-Language Foundation Model for Precision Oncology."* Nature, 1-10, 2025.

[27] G. Wang, L. Bai, J. Wang, K. Yuan, Z. Li, T. Jiang, X. He, J. Wu, Z. Chen, Z. Lei, H. Liu, J. Wang, F. Zhang, N. Padoy, N. Navab, and H. Ren, *"EndoChat: Grounded Multimodal Large Language Model for Endoscopic Surgery."* arXiv preprint arXiv: 2501.11347, 2025.

[28] H. Lai, Z. Jiang, Q. Yao, R. Wang, Z. He, X. Tao, W. Wei, W. Lv, and S. K. Zhou, *"E3D-GPT: Enhanced 3D Visual Foundation for Medical Vision-Language Model."* arXiv preprint arXiv:2410.14200, 2024.

[29] X. Wang, S. Ye, J. Feng, K. Feng, H. Yang, and H. Li, *"Performance of ChatGPT on Prehospital Acute Ischemic Stroke and Large Vessel Occlusion (LVO) Stroke Screening."* Digital Health, 10, 20552076241297127, 2024.

[30] N. V. Maiorana, S. Marceglia, M. Treddenti, M. Tosi, M. Guidetti, M. F. Creta, T. Bocci, S. Oliveri, F. Martinelli-Boneschi, and A. Priori, *"Is It Time for The Neurologist to Use Large Language Models in Everyday Practice?"* medRxiv, 2025-01, 23.25320945, 2025.

[31] D. P. Jeong, S. Garg, Z. C. Lipton, and M. Oberst, *"Medical Adaptation of Large Language and Vision-Language Models: Are We Making Progress?"* arXiv preprint arXiv:2411.04118, 2024.

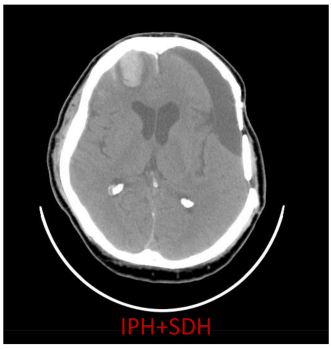
[32] P. A. Oppido, A. Fiorindi, L. Benvenuti, F. Cattani, S. Cipri, M. Gangemi, U. Godano, P. Longatti, C. Mascari, E. Morace, and L. Tosatto, *"Neuroendoscopic Biopsy of Ventricular Tumors: A Multicentric Experience."* Neurosurgical Focus, 30(4), E2, 2011.

[33] B. Wu, Y. Xie, Z. Zhang, J. Ge, K. Yaxley, S. Bahadir, Q. Wu, Y. Liu, and M. To, *"BHSD: A 3D Multi-Class Brain Hemorrhage Segmentation Dataset."* International Workshop on Machine Learning in Medical Imaging, Cham: Springer Nature Switzerland, 147-156, 2023.

[34] P. Sahoo, A. K. Singh, S. Saha, V. Jain, S. Mondal, and A. Chadha, *"A Systematic Survey of Prompt Engineering in Large Language Models: Techniques and Applications."* ArXiv preprint arXiv: 2402.07927, 2024.

[35] R. Patil, T. F. Heston, and V. Bhuse, *"Prompt Engineering in Healthcare."* Electronics, 13(15), 2961, 2024.

[36] S. M. Greenberg, W. C. Ziai, C. Cordonnier, D. Dowlatshahi, B. Francis, J. N. Goldstein, J. C. Hemphill III, R. Johnson, K. M. Keigher, W. J. Mack, J. Mocco, E. J. Newton, I. M. Ruff, L. H. Sansing, S. Schulman, M. H. Selim, K. N. Sheth, N. Sprigg, and K. S. Sunnerhagen, *"2022 Guideline for the Management of Patients With Spontaneous Intracerebral Hemorrhage: A Guideline From the American Heart Association/American Stroke Association."* Stroke, 53(7), e282-e361, 2022.



GPT-4o's answer:
1. This slice shows the supratentorial region, including the basal ganglia, frontal lobes, and lateral ventricles.

2. Yes.

3. Subdural hematoma (SDH), Intraventricular hemorrhage (IVH).

4. Subdural Hematoma (SDH): Crescent-shaped hyperdense area along the left hemisphere, between the inner table of the skull and the brain parenchyma.
Volume: Approximately 80 units.
Intraventricular Hemorrhage (IVH): Hyperdense material within the lateral ventricles (bilateral).
Volume: Approximately 15 units.

5. Subdural Hematoma (SDH):
Puncture therapy (surgical intervention) is recommended due to the significant size of the hematoma and potential mass effect.
Intraventricular Hemorrhage (IVH):
Conservative management may be appropriate unless there is evidence of obstructive hydrocephalus or elevated intracranial pressure, in which case external ventricular drainage (EVD) may be necessary.

6.Midline Shift: There is a noticeable midline shift toward the right, indicating significant mass effect from the subdural hematoma.
Ventricular Compression: The left lateral ventricle appears compressed due to the mass effect.
Effacement of Sulci: The sulci on the left hemisphere are effaced, suggesting increased intracranial pressure.

Gemini 2.0 Flash's answer:
1. This slice depicts a mid-axial section of the brain, showing the cerebral hemispheres, ventricles, and basal ganglia.

2. Yes.

3. Extradural hemorrhage (EDH) and Subdural hematoma (SDH).

4. There appears to be a small extradural hemorrhage (EDH) on the left side of the frontal region, with an estimated volume of 1000 units. There is also a large subdural hematoma (SDH) on the right side, with an estimated volume of 5000 units. The SDH is causing significant compression of the brain parenchyma and midline shift.

5. Puncture therapy.

6. There is evidence of a skull fracture on the right side. There is also significant midline shift.

Claude 3.5 Sonnet v2's answer:
1. Suprasellar axial slice showing basal ganglia level.

2. Yes.

3. Subdural hematoma (SDH).

4. Left-sided acute subdural hematoma
Thin crescent-shaped collection along left hemisphere
Estimated volume: approximately 15-20 units

5. Conservative treatment:
Close neurological monitoring
The hematoma is thin with minimal mass effect
Serial CT scans to monitor progression

6. Yes:
Minimal midline shift (<3mm)
Mild effacement of left-sided sulci
Slight asymmetry of lateral ventricles
Scalp soft tissue swelling on the left

Qwen-VL-3b-Instruct's answer:
1. The slice depicted in this image is a transverse (axial) view of the brain, showing the cerebral hemispheres and the ventricular system.

2. Yes, there is evidence of intracranial hemorrhage in this slice.

3. The observed hemorrhage subtypes are: - Subarachnoid hemorrhage (SAH) - Intraparenchymal hemorrhage (IPH)

4. Quantifying the hemorrhage volumes based on the assumption that one pixel represents a hemorrhage volume of 1 unit: - SAH: Approximately 10 units - IPH: Approximately 20 units

5. Treatment recommendation: Conservative treatment is recommended for this patient. Puncture therapy should be avoided as it could exacerbate the bleeding.

6. There are no other significant abnormalities observed in this slice.

DeepSeek-VL2-Tiny's answer:
1. The part of the brain depicted in this slice is the cerebral cortex.

2. Yes, there is evidence of intracranial hemorrhage in this slice. The presence of hyperdense areas within the brain parenchyma suggests the occurrence of hemorrhage.

3. Extradural hemorrhage (EDH), subdural hematoma (SDH), and subarachnoid hemorrhage (SAH) are observed. Intraparenchymal hemorrhage (IPH) and intraventricular hemorrhage (IVH) are not present.

4. If intracranial hemorrhage is present, the hemorrhage volume can be quantified as follows:
- Extradural hemorrhage: 1 pixel
- Subdural hematoma: 2 pixels
- Subarachnoid hemorrhage: 3 pixels
- Intraparenchymal hemorrhage: 4 pixels
- Intraventricular hemorrhage: 5 pixels

5. If intracranial hemorrhage is present, the treatment recommendation is either conservative treatment or puncture therapy. No hemorrhage is present, so no treatment is recommended.

6. No other abnormalities are observed in this slice.

LLaVA-Med-v1.5-Mistral-7b's answer:

1.

2. Yes, there is evidence of intracranial hemorrhage in this slice.

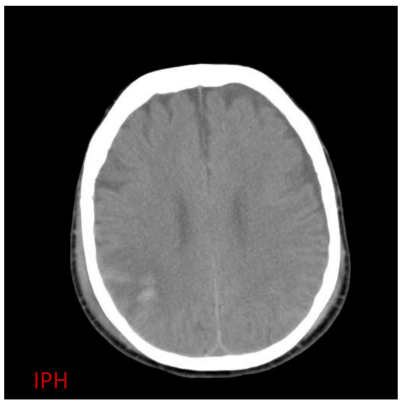
3. The image shows a subdural hematoma (SDH) and an intraparenchymal hemorrhage (IPH).

4. The SDH is located in the left frontal lobe, and the IPH is located in the left parietal lobe.

5. Conservative treatment

6. Without more information or context, it is difficult to determine if there are any other abnormalities observed in this slice.

Figure 3: Comparison of responses from six MLLMs on a random case, which illustrates a fracture in the patient's left skull due to trauma, with SDH evident in the left hemisphere and IPH in the right hemisphere.



GPT-4o's answer:

2. No.
3. No.
4. No.

Gemini 2.0 Flash's answer:

2. Yes.
3. Intraparenchymal hemorrhage (IPH)
4. Intraparenchymal Hemorrhage (IPH): There is a small area of increased density within the left parietal lobe. The estimated volume is 10 units.

Claude 3.5 Sonnet v2's answer:

2. Yes.
3. Subdural hematoma (SDH)
4. Location : Right frontoparietal convexity (crescent-shaped hyperdensity along the inner table of the skull)
Volume : Approximately 25 units (based on pixel count of the hyperdense collection)

Qwen-VL-3b-Instruct's answer:

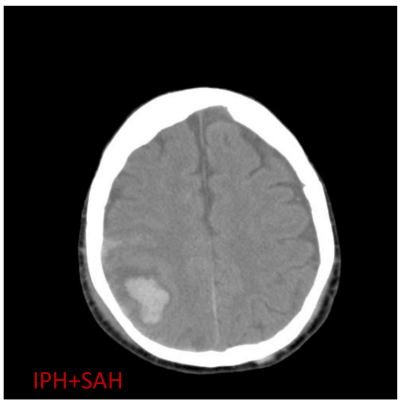
2. Yes.
3. Subdural hematoma (SDH)
4. The hemorrhage volume in the subdural hematoma is approximately 10 units.

DeepSeek-VL2-Tiny's answer:

2. Yes.
3. Extradural hemorrhage (EDH), subdural hematoma (SDH), and subarachnoid hemorrhage (SAH)
4. - Extradural hemorrhage: 1 pixel
- Subdural hematoma: 2 pixels
- Subarachnoid hemorrhage: 3 pixels

LLaVA-Med-v1.5-Mistral-7b's answer:

2. Yes.
3. Subdural hematoma (SDH) and intraparenchymal hemorrhage (IPH).
4. None



GPT-4o's answer:

2. Yes.
3. Intraparenchymal hemorrhage (IPH).
4. Location: The intraparenchymal hemorrhage is located in the left parietal lobe.
Volume: Precise quantification requires pixel-level analysis, but visually, the hemorrhage appears to occupy a small, localized region. A rough estimate would require further segmentation or pixel counting.

Gemini 2.0 Flash's answer:

2. Yes.
3. Intraparenchymal hemorrhage (IPH)
4. A hyperdense lesion consistent with IPH is located in the left parietal lobe. The hemorrhage volume is approximately 2500 units.

Claude 3.5 Sonnet v2's answer:

2. Yes.
3. Subdural hematoma (SDH)
4. Right parietal lobe IPH, approximately 3.5 x 2.5 cm in axial dimensions, estimated volume around 25-30 cc.

Qwen-VL-3b-Instruct's answer:

2. Yes.
3. - Extradural hemorrhage (EDH)
- Subdural hematoma (SDH)
4. - Extradural Hemorrhage (EDH): Approximately 10 units
- Subdural Hematoma (SDH): Approximately 8 units

DeepSeek-VL2-Tiny's answer:

2. Yes.
3. Extradural hemorrhage (EDH), subdural hematoma (SDH), and subarachnoid hemorrhage (SAH)
4. - Extradural hemorrhage: 1 pixel
- Subdural hematoma: 2 pixels
- Subarachnoid hemorrhage: 3 pixels

LLaVA-Med-v1.5-Mistral-7b's answer:

2. Yes.
3. Subdural hematoma (SDH) and intraparenchymal hemorrhage (IPH).
4. The SDH is located in the left frontal region, and the IPH is in the right parietal region.

Figure 4: Comparison of responses from six MLLMs to two slices from different layers of the same NCCT volume.

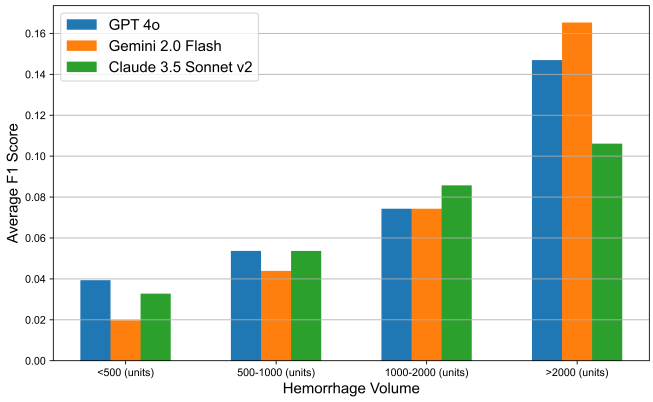


Figure 5: Statistical classification results of ICH subtypes across different hemorrhage volume ranges. The bar chart presents data for all positive cases, with the macro-averaged F1 score used for evaluation.